EFDA–JET–PR(10)19

Y Liang
and JET EFDA contributors

Overview of Edge Localized Modes Control in Tokamak Plasmas

Overview of Edge Localized Modes Control in Tokamak Plasmas

Y Liang
and JET EFDA contributors*

JET-EFDA, Culham Science Centre, OX14 3DB, Abingdon, UK

[1]Forschungszentrum Jülich GmbH, Association EURATOM-FZ Jülich, Institut für Plasmaphysik, Trilateral Euregio Cluster, D-52425 Jülich, Germany
** See annex of F. Romanelli et al, "Overview of JET Results", (Proc. 22[nd] IAEA Fusion Energy Conference, Geneva, Switzerland (2008)).*

Preprint of Paper to be submitted for publication in
Fusion Science and Technology

ABSTRACT.
The next generation of fusion machines like ITER and DEMO will need a reliable method for controlling the periodic transient expulsion of a considerable amount of energy onto the plasma facing components caused by instabilities at the plasma edge. The good plasma confinement in these tokamak devices will result in a steepened pressure profile at the plasma edge. When the pressure gradient exceeds a critical value so-called edge localized modes (ELMs) are destabilised. These modes feature a periodic fast collapse of the edge pressure, a sudden loss of the confinement and a subsequent release of heat and particles onto plasma facing components. The associated transient heat loads might cause excess erosion and lead to a strong reduction of the plasma facing components lifetime. In this paper, an overview of recent development of several ELM control methods for next-generation tokamaks, e.g. ITER is given. Some key physics issues related to the physics mechanism of ELM control are discussed.

1. EDGE LOCALIZED MODES

The discovery of the High confinement mode (H-mode), which is characterised by the formation of a transport barrier at the edge of the plasma (ETB), was made at the ASDEX Tokamak [1]. The transport barrier creates a strong pressure gradient at the plasma edge called the edge pedestal. The H-mode increases the plasma energy confinement time by around a factor of 2 compared to the Low confinement mode (L-mode). This discovery made a great step towards achieving the higher temperatures and pressures needed to create ignition conditions. The standard tokamak H-mode is foreseen as the baseline operating scenario of a future fusion machine, e.g. ITER [1]. However, as another consequence of this discovery, a steep plasma pressure gradient and associated increased current density at the edge pedestal could exceed a threshold value to drive MagnetoHydroDynamic (MHD) instabilities referred to as Edge Localized Modes (ELMs) [2, 3].

In a standard H-mode plasma, ELMs occur repetitively and the edge pedestal collapses towards a shallower pressure gradient within a few hundred microseconds. An expulsion of large amounts of heat and particles onto the plasma facing components from the confined plasma occurs and later the edge pedestal recovers again to a steeper gradient, as shown in figure 1.

Over the last two decades considerable theoretical work has been performed, both analytically and through modelling calculations, to improve their theoretical background. Ideal MHD modes driven by the steep current and pressure gradients at the edge transport barrier are regarded as the most likely candidates to explain their origin. From stability calculations performed on the basis of experimental data three types of ideal MHD instabilities can be expected at the transport barrier:

- **kink-/peeling-modes**, which are driven by the edge plasma current density, with no toroidicity dependence.
- **ballooning modes**, which are driven by the edge plasma pressure gradient, with largest amplitude on the outboard bad curvature side, and very small amplitude on the inboard side.
- **coupled peeling-ballooning modes**, which are driven by the steep edge pressure gradient and consequently large edge bootstrap current.

The development of efficient MHD stability codes such as ELITE [4, 7] and MISHKA [9] has allowed detailed quantification of peeling-ballooning stability boundaries [6] and extensive and largely successful comparisons with observation [5, 10, 8, 11].

Although some of the features are common to all ELMs, there are also distinctive differences. Regarding on the heating power dependence of the ELM frequency and the theoretical peeling-ballooning stability limit, three types of ELMs (Type-I, Type-II and Type-III) have been classified and commonly accepted [12]. Figure 2 summarizes the ELM stability diagram based on the peeling-ballooning stability limit, which depends on the maximum value of the normalized pedestal pressure gradient,

$$\alpha = -(2\mu_0=(2\pi)^2)\,/\partial V/\partial\psi(V = 2\pi^2 2R_0)\partial p/\partial\psi \qquad (1)$$

where V is the plasma volume, p is the pressure, ψ is the poloidal magnetic flux and R_0 is the major radius of the plasma, and a normalized pedestal current density j_N^{ped}, which is taken to be the peak value of the parallel current in the pedestal region normalized by the average parallel current in the pedestal.

- **Type-I ELMy**: The D-alpha radiation shows large isolated bursts and, therefore, Type-I ELMy are also called large or even giant ELMs. The plasma edge instability is close to the corner of the peeling-ballooning stability diagram or even beyond it. The instability is both pressure and edge current density driven, and as the heating power is increased, the ELM repetition frequency also increases. Type-I ELMy H-mode plasmas show a more or less strong relaxation oscillations of the edge pedestal with a low repetition frequency and have su±ciently low edge transport. no toroidicity dependence.
- **ballooning modes**, which are driven by the edge plasma pressure gradient, with The degradation of the plasma con¯nement is smaller than with other ELM types. However, the energy losses of a Type-I ELMy, ΔW_{ELM}, is also much larger than that of other ELM types, it is up to ~20% of the pedestal energy, W_{ped}. Unacceptably high transient heat loads onto the Plasma Facing Components (PFCs) are expected in a burning fusion plasma with a type-I ELMy H-mode.
- **Type-II ELMy**: Up to date, Type-II ELMy are observed only in strongly-shaped plasmas, i.e. with high elongation and triangularity of plasma cross-section. Also the plasma density needs to be rather high. The magnitude of the ELM bursts is lower and the frequency is higher than that of type-I ELMy, while the confinement stays almost as good. Sometimes, type-II ELMy are called grassy ELMs. The instability is close to the "ballooing" limit, which is pressure driven. Compared with a Type-I ELMy plasma, a enhanced magnetic turbulence has been seen in the inter-ELM phase of the Type-II ELMy H-mode plasmas. Although, the Type II-ELM has su±cient particle exhaust and tolerable transient heat loads onto the PFCs, however, it appears only in a narrow operational window, and it is still unclear whether Type-II ELMs will be possible to achieve in a burning fusion plasma. On JET, it is hard to establish a stationary pure Type-II ELMy H-mode plasma with a single null configuration, but often seen as a mixed Type-I/II ELMs in a high trangularity and high density H-mode plasmas.

- **Type-III ELMy**: The bursts are small and frequent. Therefore, another name for type-III ELMy is small ELMs. Type-III ELM appears when plasma resistivity is rather high (i.e. edge temperature rather low). The instability is close to 'peeling' limit, which is current density driven. The ELMs repetition frequency is found to decrease with the increasing heating power. Although the Type III-ELM has su±cient particle exhaust and tolerable transient heat loads onto the PFCs, however, a rather high overall energy transport leads to a stronger degradation of the energy con¯nement of the plasma compared to other ELM types.

In addition to the three conventional ELM types, there are still other different ELM types, such as compound ELMy, Type-V ELMy, observed in different devices. On NSTX, the Type-V ELMy is observed in high density, high performance discharges, and it characterized with a short-lived n = 1 pre-cursor mode rotating counter to the plasma current [14]. Although, some of the small ELM regimes identi¯ed at high collisionality, such as enhanced D_α H-mode (EDA), Type V, Type III and Type II, have been extended into lower collisionality regimes, of increasing relevance to ITER, in recent years. However, the extrapolation and uncertainty are still large, so it remains unclear whether they can be accessed on ITER.

The Type-I ELMy H-mode is foreseen as the ITER baseline scenario for the inductive operation with a fusion product of Q = 10 [1] and all scalings used for ITER design are derived mainly for this scenario. However, Type-I ELMy lead to a periodic expulsion of a considerable fraction of the stored energy content onto the PFCs, and extrapolates, based on the scaling from present tokamaks, to 15–20MJ for Type-I ELMy in ITER. This periodic and transient expulsion of energy and particles onto PFCs is too high and poses a severe problem for the integrity and lifetime of these components in ITER and future high power H-mode devices [13]. Using best estimates for divertor wetted area and in-out asymmetry, one finds that an acceptable ELM energy loss is 1MJ. This requires a decrease in the ITER natural ELM size by a factor of ~20. Therefore, reliable methods for the control of Type-I ELMy power losses are required for the steady state operation of a future fusion machine, e.g. ITER [1].

2. METHODS APPLIED FOR TYPE-I ELMY CONTROL

Several methods have been applied for Type-I ELMy control/suppression, (i) radiating divertors (impurity gas puffing) [28], (ii) magnetic triggering (vertical kicks) [22], (iii) pellet pace-making of ELMs [33], and (iv) edge ergodisation (resonant magnetic perturbation (RMP) fields) [41, 54], are presently under discussion. In the last ten years, many encouraging results has been obtained on several devices.

2.1. RADIATING DIVERTORS

Impurity gas seeding is considered as the primary technique to decrease the inter-ELM heat loads onto the divertor, and large radiation fractions in the SOL and divertor (P_{rad}/P_{out} higher than 0:5 for ITER [15] and 0.9 for DEMO [16], where P_{out} is power exhausted to the SOL) are required. On

the another hand, both increases of the ELM frequency and reduction of the ELM peak heat loads onto the divertor, so called the ELM mitigation, have been observed with impurity radiation in a Type-I ELMy H-mode plasma.

On JET, argon and nitrogen was injected in Type-I ELMy H-modes up to radiative power fractions of 65% to avoid a transition into Type III ELMy H-mode or accumulation of argon in the plasma core. The reduction of ELM energy due to radiative dissipation is about 20% on the outer divertor target and about 25% on the inner divertor target. Typically the con¯nement enhancement factor (H98(y; 2)) is decreased from 1.0 to ~0.87–0.97, depending on the radiative power fraction and the plasma density [28]. As a consequence the energy deposited onto the divertor target is then decreased. Further increase the radiative power fractions above 65%, it causes the transition from Type-I ELMy to Type-III ELMy [29, 30, 31], so called radiating Type-III ELM H-mode, and the plasma con¯nement becomes even worse (H98(y; 2) < 0.85).

In JT-60U, power handling by neon and argon seeding has been investigated in Type-I ELMy H-mode and reversed shear plasmas [17, 18, 19, 20, 21]. Good confinement (H98(y; 2) ≥ 0.85) was maintained up to a high density fraction of $\bar{n}_e/n_{GW} \sim 0.8–0.9$ (n_{GW} is the Greenwald density) and a high radiation fraction of $P_{rad}/P_{out} = 0.7–0.9$, but they were sustained for only ~2s in a standard type-I H-mode plasma. Sustainment of the high radiation plasma with the impurity seeding was also carried out in the long pulse ELMy H-mode plasma with an Internal Transport Barrier (ITB). A best performance of the energy con¯nement of H98(y; 2) = 0.95–0.88 with a large radiation fraction of 0.75¡0.95 was obtained for the combination of the Ar and Ne seeding case. Similar to the JET observations, a large radiation loss in the main plasma caused a change in the ELM characteristics from Type-I to Type-III.

On JET, it has been found that the energy loss from very small ELMs (<25kJ) only can be dissipated by radiation [28]. This is consistent with EDGE2D/EIRENE modelling, which shows that the resilient nitrogen in the divertor region gets ionized to less effective radiating higher ionization stages. Only for small ELM energies (<10kJ) is a radiative dissipation effect noticeable. So, for ITER, significant radiative dissipation of the large Type-I ELM energy is unlikely. Only for very small ELMs ($\Delta W_{ELM} < 0.6$MJ), the ELM energy loss is possibly dissipated by impurity seeding on ITER. Therefore, a combination of radiating divertor with other active ELM control methods is essential for an application for ITER.

2.2. VERTICAL KICKS

One of characteristics of Type-I ELMy is a sudden severe vertical displacement of the plasma, which may lead to loss of vertical position control. However, actively controlled vertical kicks, fast vertical movements of the plasma column, has demonstrated that the ELM frequency can be locked to the frequency of the externally imposed n = 0 magnetic perturbation, enabling ELM control (frequency and size). Here, n is the toroidal mode number. The fast modulating n = 0 magnetic perturbation is induced by a set of vertical stabilization coils with an controllable frequency and amplitude. This method was ¯rst developed in TCV [22], and has also been successfully applied in AUG [23], JET [24] and NSTX [27].

In TCV the fast vertical movement is provoked by the positional control coils inside the vacuum vessel. Experiments on the TCV tokamak showed synchronous modulation of the ELM activity, with ELMs occurring in bursts only during a rapid moving up of the plasma position approaching ~1 cm, in a single null ohmic heated type-III ELMy H- mode plasma [22]. The modulation frequency is around 50 Hz. Phase synchronization was found between the ELM cycle and the external perturbation. The ELM frequency was found to track scans in the external driver frequency about its unperturbed value over a frequency range that increased with the amplitude of the perturbation. It was also found that scaling of the ELM amplitude with the inter-ELM period was preserved in the presence of the perturbation, so that the ELM amplitude can be controlled by altering the ELM period. In NSTX, external coils are used and can increase the ELM frequency by a factor of two. Similar to TCV results, ELMs are most likely to be triggered as the plasma moves up by ~2cm [27].

DINA simulations showed that when the phase locked, the ELMs were found to occur at times when the edge current density was increased under the action of the perturbation, either by direct induction from the changing current in the coil, or by movement of the plasma through the vacuum field[22]. Triggering ELMs with vertical kicks in a ELM-free phase has also been demonstrated on TCV in a double null Ohmic heated H-mode plasma. This methods has been used to feed back control the plasma density rise and impurity accumulation associated with an ELM-free H-mode discharge. Therefore, it was considered that the ELMs could indeed be driven unstable by the rapid moving up of the plasma position with a modulation of the n = 0 magnetic perturbation, attributed to the increased edge current destabilizing the peeling mode (current-driven modes).

On AUG, active ELM control with vertical kicks has now also been demonstrated in the ITER-relevant type-I ELMy regime [23]. The experiments showed the ELM frequency becoming identical to the driving frequency in steady state for an applied motion of only about twice the value caused by an intrinsic ELM event. Figure 3 shows a typical example from this experiment. The ELM frequency is raised and locks to the frequency of imposed vertical (position z; $v \equiv dz/dt$) movement of the plasma column. The modest impact of magnetic triggering on particle and energy confinement has been seen when the ELM frequency increase from 43 to 56Hz. A reduction of ELM-imposed energy losses is also visible. It was found that ELMs were triggered when the plasma downshift velocity reached its maximum, corresponding to the lowest edge current value. The triggered ELMs show clear type-I features. This is the opposite behaviour expected from the peeling-ballooning nature attributed to the ELM boundary and to TCV observations. The reason for this behaviour is not yet clear. The fact that magnetic ELM triggering was obtained at AUG in the type-I ELMy H-mode raises the question of the underlying ELM physics.

Recently, ELM control with vertical kicks has been successfully applied in JET [24, 25]. The fast plasma vertical movement is controlled by the vertical stabilization controller, which has been modi¯ed to allow the application of a user defined voltage pulse (so called kick) at an adjustable frequency. Presently, a maximum value of the kick frequency is up to ~60Hz which is due to technical constraints. Similar to the results observed from AUG, JET experimental results show that plasma kicks moving the plasma down towards the X-point can generate high frequency,

synchronous ELMs in standard Type-I ELMy H-modes. With an application of the vertical kicks the pedestal density reduces by ~20% when the ELM frequency is increased from 15Hz to 40Hz,while the modest impact on the pedestal temperature are seen. This causes the edge pressure gradient being reduced. The reduction in ELM size (up to a factor of 3) is accompanied by a minor (<10%) reduction of the stored energy. One also found that a minimum kick size is necessary for the trigger to occur. Successful ELM triggering is obtained in JET with displacements of the current centroid ~0.5–1.5cm and velocities in the order of 5–10m/s. Those values still remain less than twice of the plasma displacement caused by intrinsic ELMs. However the fast plasma movement is not the only requirement for the ELM to be triggered. For similar pre-programmed kicks the plasma response depends also on the local plasma parameters. Typically 2–3ms delays are observed between the start of the kick and the ELM and the delays are slightly higher for plasmas with higher pedestal temperature. An increase in the edge temperature will increase the current penetration time. This observation indicates that the modi¯cation of edge currents by the induced field and/or change in the plasma equilibrium might be the possible role for the ELM trigger. To date, the precise physics mechanism is still unknown.

2.3. PELLET PACE-MAKING OF ELMS

Shallow injection of pellets has been thought to be a tool to increase the Type-I ELMy frequency to the pellet injection rate, so called pellet pace-making of ELMs, and consequentially reduce the power load per ELM on the divertor target. Following pioneering experiments on AUG [32], this method has been also studied on JET [35] and DIII-D [36], and it is considered as one of potential tools for ITER ELM control [38].

On AUG, the feasibility of ELM control by continuous injection of small frozen deuterium pellets from the high ¯eld side into H-mode discharges has been demonstrated [32]. Two examples with (Pulse No: 15420) and without (Pulse No: 15520) pellet injection are shown in Fig.4. In this experiment, a pellet velocity of 560ms^{-1} and a size of about 6×10^{19} D-atoms were selected. A moderate repetition rate close to 20Hz was chosen to avoid over-fuelling of the core plasma. ELMs were triggered in less than 200μs after pellet arrival at the plasma edge, at which time only a fraction of the pellet has been ablated, forming a rather localized, three-dimensional plasmoid, which drives the edge unstable well before the deposited mass is spread toroidally. The most probable location of the seed perturbation was found to be at the middle of the pedestal at the high plasma pressure gradient region. The onset of the MHD signature of the ELMs was detected about 50¹s after the pellet reached the seed position [34]. The ELM frequency is increased and controlled to the imposed pellets injection frequency. Moreover, the impact of the high frequency triggered ELMs on plasma density and stored energy is obviously smaller.

Further experiments on AUG also demonstrated that a over-fuelling of core plasma with either a high pellet injection frequency or a large pellet size could cause enhancement of the convective energy losses and then impact on the energy confinement[33]. One example from this experiment is shown in Fig.5. Besides a clear enhancement of the density level, a tendency towards a reduced

confinement and enhanced ELM frequency with respect to the pre-pellet phases is visible. Clearly, pellets are still causing some fuelling and also a reduction in con¯nement. Hence, pellet injection for ELM pacing should use the smallest possible pellets and a shallow injection. It is still to be proven whether the concept will also work for bigger machine sizes.

A step forward in this mission was achieved on JET. Although the experiments were performed in a parameter regime (pellet sizes of ~4 mm (about 4×10^{21} D atoms) and injection velocities of 150–300 m/s) unsuitable for pellet ELM pacing both with respect to pellet frequency and size they demonstrated that prompt triggering of ELMs takes place at JET as well [35]. It was found that despite the fuelling effects of the large pellets, ELMs are triggered at any time in the ELM cycle. Only a minor amount of a fuelling sized pellet mass is ablated during the penetration of the plasma up to the pedestal top, triggering the ELM. The pellet triggered ELM appears not to be different from an intrinsically occurring one in terms of energy loss. However, a reduced pellet mass is expected to cause a reduced ablation rate. Hence a lower radial velocity of the pellet might be required to increase the perturbation at the pedestal, if the ablation rate of the small pellets becomes too low. A reduced pellet radial velocity can be achieved by a reduced launch velocity and a change in the inclination angle of the trajectory. The JET experimental results also demonstrate the benefits for high field side pellet injection: the penetration to the pedestal top is achieved with a lower pellet mass.

A pellet dropper ELM triggering tool has been developed for testing the ability of small slow pellets to achieve ELM pacing on the DIII-D tokamak [37]. The pellet dropper has obtained 50Hz injection rate and 1 mm pellet size. Since pellets are dropped into a funnel that guides them into a tube directed to the top of the plasma using gravity as the accelerator, it results in slow injection speed, $< 10\mathrm{ms}^{-1}$, to minimize penetration into the core plasma. Initial results with the pellet dropper indicate that fast ions deflect the pellets toroidally before penetrating deep enough to trigger ELMs [36]. The pellet location as a fraction of the pedestal height is plotted as a function of the pedestal temperature in Fig. 6 for some different operational conditions. It has been found that the ELMs are triggered well before the fueling pellet reaches half way up the pedestal. This is somewhat in contrast to the measurements from AUG where it was observed that HFS injected pellets needed to penetrate beyond this depth to trigger an ELM [34]. Although a pellet dropper type device is not directly suitable for ITER due to lack of vertical injection/dropping ports. Future results from the dropper on DIII-D will be used to help extrapolate the minimum pellet size and speed needed to reliably trigger ELMs in ITER.

Progress in understanding the physics of pellet-triggered ELMs is emerging from simulations using the nonlinear MHD code, JOREK [39]. The simulation of pellets injected in the H-mode pedestal shows that high pressure develops in the high density plasmoid, in this case the maximum pressure is ~5 times the pressure on axis. There is a strong initial growth of the low-n modes followed by a growth phase of the higher-n modes ballooning like modes. The coupled toroidal harmonics lead to one single helical perturbation centred on the field line of the original pellet position as seen in Fig.7, and there is some experimental evidence for this from JET and DIII-D.

With respect to ITER, the tool is still to be investigated in the relevant parameter region of,

e.g. less collisionality or much higher pedestal temperature. Also, an enhancement factor of the intrinsic ELM frequency by a factor of almost 20 is necessary. On the other hand, synergism of pellet fuelling and external ELM triggering seems quite possible. In addition, a question, whether alternative materials for pellets could be used for ITER ELM control, is under consideration. However, indeed, pellet pace-making could even assist other ELM control techniques, helping to compensate the density pump-out caused by RMP ELM control/suppression.

2.4. RMP ELM CONTROL/SUPPRESSION

Active control of ELMs by RMP fields offers an attractive method for next-generation tokamaks, e.g. ITER. The recent obtained results from DIII-D, JET, MAST, and NSTX tokamaks have shown that magnetic field perturbations can either completely suppress ELMs [41], trigger small ELMs during ELM free periods or affect the frequency and size of the type-I ELMy in a controllable way, preserving good global energy confinement [54, 69, 71].

2.4.1. ELM suppression with RMP

Up to date, there is only one successful demonstration of the ELM suppression technique reported from DIII-D, where the In-vessel Coils (I-coils) have been employed. The I coil consists of 12 single-turn loops, six above and six below the midplane (up-down symmetric) mounted on the low field side of the vessel. For the ELM suppression experiments, the upper and lower loops are operated with opposite current polarities (odd parity), and induce a static perturbation field with a toroidal mode number n = 3. The experimental results show a collisionality dependence of ELM control/suppression with n = 3 fields. Complete ELM suppression with stationary densities and radiated power maintained for 17 energy confinement times has been obtained in low collisionality ($\nu^*_e \leq 0.2$) H-mode plasmas with application of an n = 3 field [41]. However, in high collisionality ($\nu^*_e \approx 1$) plasmas [40], Type-I ELMy are replaced by small intermittent events with a coherent amplitude modulation of 130Hz during application of the n = 3 filed. The influence on the ELMs in those experiments are only observed in a narrow q_{95} window ranging from 3.5 to 3.9 with an odd parity n = 3 field and ~7.2 with a even parity n = 3 field. Outside this q_{95} range there is little or no effect on the ELMs indicating a resonant condition on the amplitude and con¯rming the requirement for pitch alignment of the perturbation fields.

Further more, ELM suppression with n = 3 fields has been also observed in a ITER Similar Shaped (ISS) high triangularity ($\delta = 0.53$) plasma with ITER relevant collisionalities $\nu^*_e \leq 0.2$ [42]. A example discharge with a q_{95} scan from this experiment is shown in Fig.8. In ISS plasmas, the minimal coil current required to suppress ELMs is approximately 25% higher than in low average triangularity plasmas. It is also found that the width of the resonant q_{95} window (from 3.52 to 3.62) observed for ELM suppression is smaller in ISS plasmas than in low average triangularity plasmas. An analysis of the positions and widths of resonant magnetic islands across the pedestal region, neglecting resonant field screening or a self-consistent plasma response, indicates that di®erences in the shape of the q profile may explain the need for higher RMP coil currents during ELM suppression in ISS plasmas.

RMP effects on the pedestal profiles has been studied for comparing ELM suppression with stability theory on DIII-D [42]. Figures 9 show a comparison of the ELM behaviour and pedestal profiles with various I-coil currents in ISS plasmas. As the I-coil current is increased there is a strong monotonic reduction in the pedestal density and the edge toroidal rotation increases with each step in the I-coil current. The change in ion temperature is most pronounced when going from 0 to 4kA, particularly in the high gradient region, and drops slightly at the top of the pedestal when going from 4 to 6.3kA. The electron temperature profile shows a steady reduction in pedestal width and height with increasing I-coil current. The full ELM suppression occurs when the pressure gradient pro¯le resides when the I-coil currents is above 4kA. This result suggest that the critical region required for ELM stabilization lies between $\Psi_N \sim 0.80-0.97$, where Ψ_N is the normalized flux. This change in the pressure profile moves the pedestal into a stable peeling-ballooning mode operating region as seen in Fig. 10 [41]. This result suggests that ELM suppression occurs in this case without the RMP directly interacting with the ELM eigenmode.

Compensation of the density pump out with additional fuelling has been preformed during DIII-D ELM suppression experiments. Partially compensation of density pump-out during RMP ELM suppression can be archived by means of gas puffng. However, strong fuelling with gas puffng or with pellets injection could bring small ELMs back.

One example has been shown in Fig.11. Thus further optimization of the RMP technique is needed to be able to fully suppress ELMs during pellet fueled H-mode scenarios for application to ITER [36].

To date, many attempts to model ELM suppression/control have focused on the idea that a RMP field penetrating into the edge plasma region would interact with the plasma equilibrium field to produce an outer 'ergodic' magnetic field structure. This would enhance edge thermal and particle losses, weaken the edge transport barrier and its gradients, and thus reduce the peeling-ballooning instabilities thought to underlie ELM formation [49, 51, 41]. This mechanism is mainly supported by two experimental evidences from DIII-D: i) splitting of the inner strike-point observed during RMP ELM suppression phase [46, 47]; and ii) spin-up of edge plasma rotation in co-current direction and charging of the plasma edge electric field to more positive due to larger losses of electrons than ions with an ergodic boundary [48]. However, an objection to this interpretation is that either bulk plasma or diamagnetic rotation [52, 53] can screen the RMP fields from the plasma whenever they encounter a resonant surface. Furthermore, it is important to note that many calculations of the Chirikov parameter [50] model the plasma as producing a vacuum response to the RMP, and the resulting total field will not be in magnetostatic equilibrium. Here, the Chirikov parameter (σ), which is a measure of magnetic island overlap, is used to de¯ne the stochastic layer as the region for which σ is greater than 1.

Recent experimental results from ELM suppression in Hybrid H-mode plasmas on DIII-D show that small ELMs can appear when the edge safety factor is outside the resonance window or when the H-mode pedestal is perturbed, which are not related to P-B stability [45]. This result indicates that a 3D equilibrium modification may important for understanding the effect of RMP on the edge pedestal stability [75]. On other hands, changes in the edge-plasma profiles during the RMP ELM

suppression phase are indicative of a signi¯cant alteration in the particle balance with a relatively small change in the energy transport and can not be explained by stochastic transport theory.

Based on the results from DIII-D, the criteria for ELM suppression with RMP requires the Chirikov parameter number at the plasma edge layer ($\sqrt{\Psi} \geq 0.925$) larger than 1 [49], and it has been applied for a design of the ITER ELM control coils. However, in DIII-D a single row of off-midplane in-vessel coils did suppress ELMs [43]. The perturbation spectrum induced by a single row of coils is different to that with both up-down coils. In addition, recent experimental results from both MAST (n = 3, in-vessel off-middle plane coils) [69] and JET (n = 1 and 2, external middle plane coils) [54] show that ELM suppression can not been achieved even with a Chrikov parameter larger than 1 at $\sqrt{\Psi}_{pol} > 0.925$. Those results suggest that ELM suppression using the RMP may also depends on the perturbation spectrum (not only the mode number, but also the ratio of the resonant to the non-resonant components). Although complete ELM suppression with RMP is only obtained on a single device (DIII-D), application of RMPs on ther machines has either triggered ELMs in otherwise ELM free H-mode periods or increased the ELM frequency in regularly ELM-ing discharges.

2.4.2. Active ELM control with RMP

Recent experiments on JET have shown that type-I ELMy can be actively controlled by application of static low n = 1 or 2 external magnetic perturbation fields produced by four external Error Field Correction Coils (EFCC) [61] mounted far away from the plasma between the transformer limbs [54, 55, 56, 58]. An overview on an JET ELM control pulse is shown in Fig.12. In these experiments, the type-I ELMy H-mode plasma with a high triangularity shape ($\delta_U = 0.45$ and $\delta_L = 0.4$) was sustained by neutral beam injection. The electron collisionality at the pedestal is ~0.2. The Chirikov parameter calculated using the experimental parameters and the vacuum approximation of the perturbation field is about 0:85 at $\Psi^{1/2} = 0.95$. During the EFCC phase the D_α signal measuring the ELMs showed a strong reduction in amplitude. The ELM frequency increased from ~30Hz to ~120Hz, while the periodic energy loss due to the ELM crashes normalized to the total stored energy, $\Delta W/W$, measured by a fast diamagnetic loop, indicates a strong reduction from ~8% to values below the noise level (< 2%) of the diagnostic. A modest drop (a few per cent) in the total stored energy has been observed during the ELM control phase with the EFCCs. However, when normalised to the IPB98(y; 2) scaling the con¯nement time shows almost no reduction.

The electron density at the pedestal top decreases by ~20% due to so called density pump-out [60] during the application of the n = 1 field, while the pedestal electron temperature increased what kept the pedestal pressure almost constant. However, the pedestal pressure gradient obtained from the derivative of the fitted curve shows that the maximum pressure gradient in the profile is decreased by 20% during the application of the n = 1 field, and the edge pressure barrier is 20% wider [64]. This is an effect mostly ascribable to the strong decrease in ne pedestal height with an almost unvaried width. The minimal amplitude of perturbation ¯eld required for an increase in ELM frequency, so called ELM mitigation threshold, has a higher value than the density pump-out threshold. In addition, previous JET experimental results also show that the ELM mitigation

threshold increased with decreasing q_{95} [55]. Stability analysis of controlled ELMs suggests that the operational point with n = 1 perturbation ¯eld moves from the intermediate-n peeling-ballooning boundary to the low-n peeling boundary, and the radial width of the most unstable mode reduced from ~3% down to ~1% of the normalised minor radius [62].

Reduction of both, the peak particle and the peak heat °uxes during the ELM crash, have been observed in ELM control experiments with application of an n = 1 field [56, 58, 63]. The heat °uxes were measured by Langmuir probes embedded in the divertor tiles and a fast IR camera viewing the divertor target plates. The reduction in heat °ux is mainly due to the drop of particle °ux rather than the change of the electron temperature. A reduction in the particle °ux has also been observed on the outboard down of IEFCC which could be due to a hysteresis e®ect or non-stationary nature of the experiment.

Active control of type-I ELMy with n = 1 fields has been developed toward more ITER-relevant configurations and parameters in a wide operational space of plasma triangularity (δ up to 0:45), q_{95} (3−4.8) and normalised beta (β_N up to 3.0) [55, 65]. A similar wide operational window of q95 has also been obtained for ELM control with n = 2 fields [55].

Similar plasma braking effects have been observed with n = 1 and n = 2 external fields when the same EFCC coil current was applied [57]. The torque profile induced by the n = 1 field has been measured, and it has a global profile. The maximal value of this torque is at the plasma core region and it is about half of the neutral beam injection torque. The calculation shows that the plasma is mainly in the ν regime in the plasma core, but is close to the transition between the 1/ν and νregimes. A discrepancy between the observed torque and the torque predicted by the Neoclassical Toroidal Viscosity (NTV) theory has been found. Although, both the boundary layer effect and using the Largrangian variation of the magnetic field strength can reduce this discrepancy. However, the magnitude of the NTV torque calculated in the ν regime is still at least one order smaller than the observed one [66, 74].

The compensation of the density pump-out has been demonstrated using either gas fuelling or pellets injection in low triangularity H-mode plasmas [57, 56, 58]. Although the ELM frequency stays high with n = 1 fields, however, no recovery of stored energy was observed. An optimised fuelling rate to compensate the density pump-out effect has been identified, and it depends on the plasma configuration.

On JET, although the calculation of the perturbed separatrix topology with a vacuum condition suggested that a splitting of the strike point at the inner divertor with n = 1 and n = 2 fields on JET, however, no any evidence of the splitting of either heat flux and particle flux has been observed even when the reduction of ELM size and increase of ELM frequency have been clearly seen in H-mode plasmas [58]. On the other hand, complete ELM suppression as reported by DIII-D has not been achieved on JET up to date.

Multiple resonances in the Edge Localized Mode (ELM) frequency (f_{ELM}) as a function of the edge safety factor q_{95} have been observed for the first time with an applied low n (=1,2) field on the JET tokamak [59]. Without an n = 1 field applied, fELM increases slightly from 20 to 30 Hz

by varying the q_{95} from 4 to 5 in a type-I ELMy H-mode plasma. However, with an n = 1 field applied, a strong increase in fELM by a factor of 4–5 has been observed with resonant q_{95} values, while the fELM increased only by a factor of 2 for non-resonant values. The Chirikov parameter calculated using the experimental parameters and the vacuum approximation of the perturbation field indicates that the ergodisation zone may only appear at the far plasma boundary ($\sqrt{\Psi} > 0.95$). The mechanism of edge ergodisation, which is used to explain the results of the ELM suppression with n = 3 field on DIII-D, may explain the global effect of the n = 1 field on f_{ELM} on JET, but it cannot explain the multi-resonance effect observed with the low n fields. A model, which assumes that the ELM width is determined by a localised relaxation triggered by an unstable ideal external peeling mode, can qualitatively predict the observed resonances when low n fields are applied [67].

On MAST, experimental results show that ELMs can be triggered in a non-steady state ELM-free regime by applying n = 3 RMP fields, which provides density control [69, 70]. Similar results are also observed on NSTX. The application of n = 3 static RMP fields from external coils can trigger ELMs in an otherwise non-steady state ELM- free discharge, again providing some density control [71]. The ELM frequency increases with RMP coil current.

An additional advantage of RMP coils is that they could also provide a technique for ELM pacing. Experiments on NSTX show reliable ELM triggering each time the n = 3 RMP coil current is pulsed, with no apparent loss of stored energy [72]. Similar results are also observed on DIII-D, which demonstrated a factor of two increase in the ELM frequency could be achieved. However, at the higher ELM frequencies, it appears that the triggered ELM energy loss is not inversely proportional to the ELM frequency.

Although the mechanism of the ELM control with RMP is not fully understood yet, however, it has been examined in a wide operational window in many different devices. Further optimisation of the magnetic perturbation with less reduction of the plasma performance and understanding the unlaying physics are essential for the future investigations.

2.4.3. Future RMP ELM control/suppression experiments

The coil systems in different devices employ differing designs, e.g. internal off-midplane coils (DIII-D, MAST) and external midplane coils (JET, MAST, NSTX), and provide different poloidal, m, and toroidal, n, mode number spectra as well as differing radial profiles. Nevertheless, there are common observations like plasma density pump-out and magnetic rotation braking. To date, complete ELM suppression has only been achieved within an operational window of $q_{95} = 3.4 \pm 0.2$ by using n = 3 fields induced by internal off-midplane coils in DIII-D. Guided by the DIII-D results, a set of ELM control coils has been designed for ITER [49].

To provide a more reliable method for ELM control/suppression, lots of ongoing e®orts are presently contributing on two major topics: **application** and **physicsmechanism**.

- **Application**: This includes i) the influence of RMP on the ELM frequency and size, ELM peak heat loads, plasma confinement; ii) operational window, which is defined by the locked mode threshold and minimal perturbation necessary for increase of ELM frequency; iii) rotation

braking with magnetic perturbations; iv) density dump-out compensation; v) application for ITER-like scenarios.

- Physics mechanism: This includes i) field penetration process including edge ergodisation, field screening by plasma rotation and 3D equilibrium effect; ii) ELM stability; iii) Dynamics of edge pedestal profiles; and iv) multi-resonance effect.

To investigate the physics mechanism of RMP ELM control/suppression, several new RMP coil systems on the world's tokamaks are planned. DIII-D will install 48 new coils (4 rows, and each row has 12 coils) on the inboard wall [44]. This system is very flexible for adjusting the perturbation spectrum. The maximal toroidal mode number of the perturbation fields can be up to 6. MAST will double the number of coils in the lower ring to 12, then a perturbation field with a toroidal mode number up to 6 can be induced, and a better scan of perturbation spectra for ELM suppression can be carried out. On AUG, a set of 3×8 ELM control coils including a capability to rotate the perturbation up to n = 3 is presently installed [73]. Two rows of internal coils above the mid-plane are being considered for JET (one with 8 coils, the other with 24) [68]. This system is flexible enough to be able to independently adjust both the Chirikov parameter and the magnetic perturbation spectrum in ITER-relevant scenarios. NSTX is also considering two rows of internal coils above and below the mid-plane, each one having 12 coils. Future experiments from those devices o®er the possibility to examine the underlying mechanism of complete ELM suppression and ELM control.

2.5. COMBINATION OF DIFFERENT METHODS

To gain a higher fusion energy production and to secure the plasma first wall components, a fusion device, i.e. ITER, needs to be operated in a high density (close to greenwald limit), high edge radiation and steady state small ELMs or ELM-free regime. this may need a combination of several di®erent methods for the large ELM control/supprssion.

On JET, the preliminary experimental results show that the combined application of n = 1 field and vertical kicks (n = 0) leads to a reduction of the threshold perturbation level necessary for the ELM mitigation to occur [26]. It could reduce the technical diffculty to access a further high ELM frequency control with a safe size of vertical kicks.

Successful ELM control with a combination of n = 1 filed and pellet injection has been demonstrated on JET. The ELM frequency can be increased without any drop of plasma density. During application of the n = 1 field, ELM frequency increase, even though some of ELMs are triggered by pellet injection. Further RMP ELM control experiments with a radiating divertor are planned.

SUMMARY

Erosion and damage caused by large ELMs is a major hurdle on the route towards achieving magnetic fusion in a reactor scale machine. Scaling predicts that the large ELM energy in ITER will exceed the acceptable level by a factor of ~20. A reliable ELM control method is needed.

In the past years, several ELM control/suppression methods are developed. Some important

results are summarized below:

- Combination of radiating dervertor with other active ELM control methods is essential for an application for ITER. Radiating type-III ELM is successful ELM control, but full H-mode confinement has still to be demonstrated.
- Vertical kicks need in-vessel coils to reach a high kick frequency. The recent results from JET are promising, and this technique will be used for ITER-like wall experiments on JET, in which case the ELM size need only to be reduced by a factor of ~2–3.
- Pellet pacing can typically achieve a factor of two reduction in the energy per ELM. A high frequency ELM pacing still needs to be demonstrated on JET. Also, for ITER the reliability of a pellet system has to be questioned. Indeed, pellet pace-making could assist other ELM control techniques, helping to compensate the density pump-out caused by RMP ELM control/ suppression.
- RMP ELM suppression/control shows very promising results up to now, although, the physics mechanism is not well understood yet. Future joint experiments from different devices (DIII-D, JET, MAST, NSTX, AUG,) will help to understand physics and support for ITER. ITER may need combination of different ELM control methods, which is still under investigation.

ACKNOWLEDGEMENT

This work, supported by the European Communities under the contract of Association between EURATOM and FZJ, was carried out within the framework of the European Fusion Development Agreement. The views and opinions expressed herein do not necessarily re°ect those of the European Commission.

REFERENCES

[1]. ITER Physics Basis, 1999, Nuclear Fusion **39** 2137
[2]. Wagner F, et al 1982, Physical Review Letters **49** 1408
[3]. Connor J.W, 1998, Plasma Physics and Controlled Fusion **40** 531
[4]. Snyder P.B, et al 2002, Physics of Plasmas **9** 2037
[5]. Snyder P.B and Wilson H R, 2003 Plasma Physics and Controlled Fusion **45**, 1671
[6]. Snyder P.B, et al 2004 Nuclear Fusion **44**, 320
[7]. Wilson H.R, et al 2002 Physics of Plasmas **9**, 1277
[8]. Saarelma S, et al 2003 Nuclear Fusion **43**, 262
[9]. Huysmans G.T.A, Sharapov S.E, Mikhailovskii A.B, and Kerner W, 2001 Phys. Plasmas 8, 4292
[10]. Mossessian A, et al 2003 Physics of Plasmas **10**, 1720
[11]. Lao L.L, et al 2001 Nuclear Fusion **41**, 295
[12]. Zohm H, 1996, Plasma Physics and Controlled Fusion **38** 105
[13]. Loarte A, et al 2003, Journal of Nuclear Materials **313-316** 962
[14]. Maingi R. et al 2005 Journal of Nuclear Materials **337-339** 727-731

[15]. Shimada M. et al 2007 Progress in the ITER Physics Basis: chapter 1. Overview and summary Nuclear Fusion **47** S1
[16]. Tobita K. et al 2009 Nuclear Fusion **49** 075029
[17]. Itami K. et al 1999 Journal of Nuclear Materials **266-269** 1097
[18]. Sakurai S. et al 2001 Journal of Nuclear Materials **290-293** 1102
[19]. Kubo H. et al 2001 Nuclear Fusion **41** 227
[20]. Kubo H. and the JT-60 Team, 2002 Physics of Plasmas **9** 2127
[21]. Higashijima S. et al 2003 Journal of Nuclear Materials **313-316** 1123
[22]. Degeling A.W., et al 2003 Plasma Physics and Controlled Fusion **45**, 1637.
[23]. Lang P.T., et al , 2004 Plasma Physics and Controlled Fusion **46**, L31-L39
[24]. Sartori F., et al 35th EPS Conference, Crete, Greece (2008)
[25]. de la Luna E. , et al 36th EPS Conference, Sofia, Bulgaria. (2009)
[26]. de la Luna E. , et al 51st APS conference, Atlanta GA, USA (2009)
[27]. Gerhardt S, et al ITPA PEP meeting in Naka, 2010.
[28]. P. Monier-Garbet et al 2005 Nuclear Fusion, **45**, 1404.
[29]. Sartori R. et al 2004 Plasma Physics and Controlled Fusion, **46**, 723.
[30]. Rapp J. et al 2004 Nuclear Fusion, **44**, 312.
[31]. Rapp J. et al 2005Journal of Nuclear Materials, **337-339**, 826.
[32]. Lang P.T., et al , 2003 Nuclear Fusion **43** 11101120
[33]. Lang P.T., et al , 2004 Nuclear Fusion **44**, 665
[34]. Kocsis G., et al 2007 Nuclear Fusion **47** 11661175
[35]. Lang P.T., et al 2007 Nuclear Fusion **47** 754761
[36]. Baylor L.R. et al 2008 Proc. 35th EPS Conf. on Plasma Physics (Hersonissos, Greece) vol 32D (ECA) P4-098
[37]. Combs S.K. et al 2007 Proc. 22nd Symp. on Fusion Engineering (Albuquerque, NM, USA) IEEE Cat. #07CH32901C http://ieeexplore.ieee.org/xpl/conferences.jsp
[38]. Polevoi A.R. et al 2003 Nuclear Fusion **43** 1072.
[39]. Huysmans G.T. A., et al 2009 Plasma Phys. Control. Fusion **51** 124012
[40]. Evans T, et al 2004, Physical Review Letters **92** 235003
[41]. Evans T, et al 2006, Nature Phys. **2** 419
[42]. Evans T.E. et al 2008 Nuclear Fusion **48** 024002
[43]. Fenstermacher M.E. et al 2008 Nuclear Fusion **48** 122001
[44]. Fenstermacher M.E. et al 2009 18th PEP ITPA Mtg. PPPL Princeton, NJ October, 5-7
[45]. Hudson B. et al 2010 Nuclear Fusion **50** 045006
[46]. Jakubowski M, et al 2006, PRL **96** 035004
[47]. Schmitz O, et al 2008, Plasma Physics and Controlled Fusion **50** 124029
[48]. Burrell K. et al 2005, Plasma Physics and Controlled Fusion **47** B37
[49]. Schaffer M.J., et al 2008 Nuclear Fusion **48**, 024004
[50]. B.V. Chirikov, Physics Reports **52**, 263 (1979).

[51]. Bècoulet M. et al 2008 Nuclear Fusion **48** 024003
[52]. M. Heyn et al Nuclear Fusion **48**, 024005 (2008).
[53]. R. Fitzpatrick, Nuclear Fusion, **33**, 1049 (1993).
[54]. Liang Y, et al 2007, Physical Review Letters **98** 265004
[55]. Liang Y, et al 2007, Plasma Physics and Controlled Fusion **49** B581
[56]. Liang Y, et al 2009, Journal of Nuclear Materials **390-91** 733-739
[57]. Liang Y. et al 2010 Plasma and Fusion Research, accepted
[58]. Liang Y. et al 2010 Nuclear Fusion **50** 025013
[59]. Liang Y. et al 2010 submmitted to Physical Review Letters
[60]. Vallet J C, et al 1991 Physical Review Letters **67** 2662
[61]. Barlow I, et al 2001, Fusion Engineering Design **58-59** 189
[62]. Saarelma S, et al 2009 Plasma Phys. Control. Fusion **51** 035001
[63]. Jachmich S, et al 2007 Proc. 34th EPS Conf. on Plasma Physics (Warsaw, Poland) P5.099
[64]. Al¯er A, et al 2008 Nuclear Fusion **48** 115006
[65]. Koslowski H R, et al 34th EPS Conference on Plasma Phys. Warsaw 2-6 July 2007, ECA Vol. 31F, P-5.135 (2007)
[66]. Sun Y, et al 2010, Plasma Physics and Controlled Fusion accepted
[67]. C. G. Gimblett, R. J. Hastie and P. Helander, Physical Review Letters, **96**, 035006-1-4 (2006).
[68]. Lowry C.G. et al 2009 American Physical Society, 51st Annual Meeting of the APS Division of Plasma Physics, November 2-6, #UP8.089
[69]. Krik A, et al 2010 Nuclear Fusion **50** 034008
[70]. Nardon E. et al 2009 Plasma Physics and Controlled Fusion **51** 124010
[71]. Canik J.M., et al 2010 Nuclear Fusion **50** 034012
[72]. Canik J.M., et al 2010 Nuclear Fusion **50** 064016
[73]. Suttropa W., et al 2009 Fusion Engineering and Design **84** 290294
[74]. Shaing K C, 2003 Physics of Plasmas **10** 1443
[75]. Park Jong-kyu, 2007 Physical Review Letters **99**, 195003

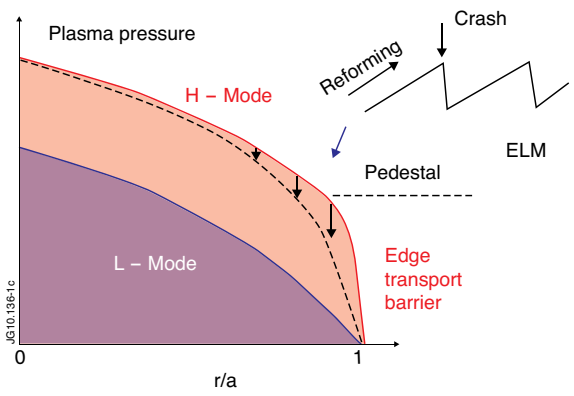

Figure 1: Pressure profiles of L and H- Mode plasmas.

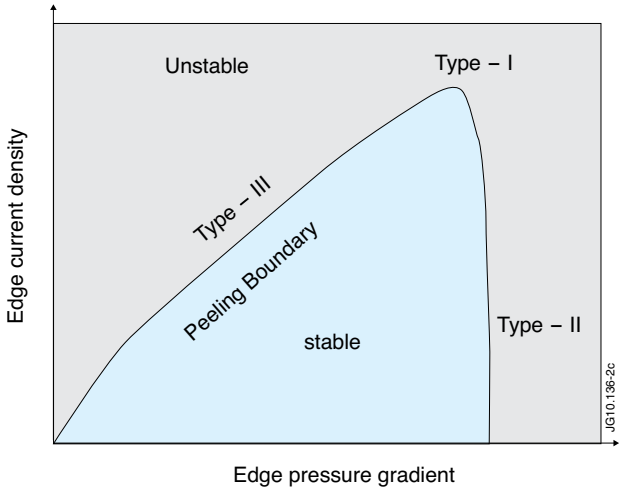

Figure 2: ELM stability diagram.

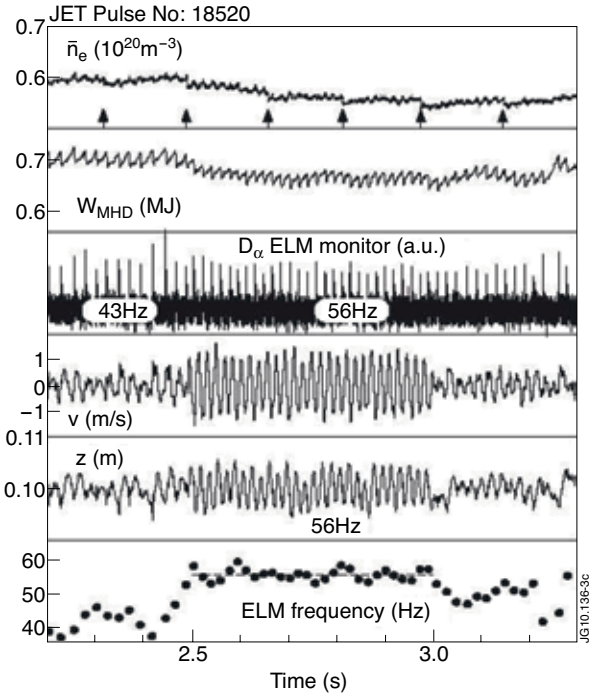

Figure 3: Demonstration of magnetic ELM triggering in a type-I ELMy H-mode. From reference [23].

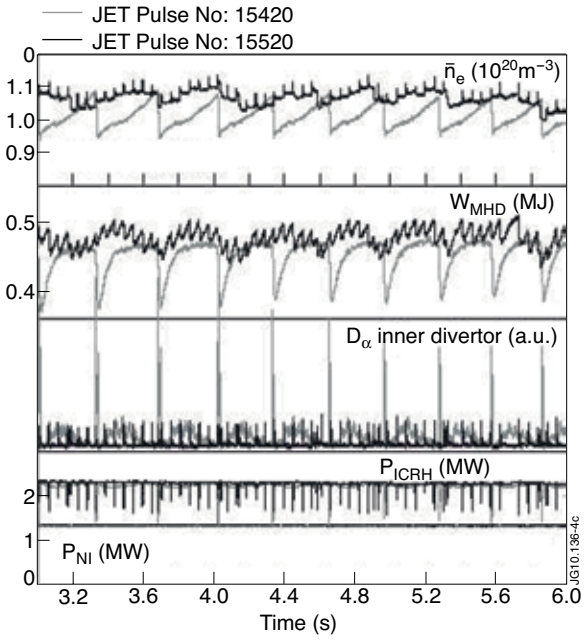

Figure 4: Global temporal evolution of identical discharges without (Pulse No: 15420, grey) and with (Pulse No: 15520, black) pellet forced ELM control on AUG. From reference [32].

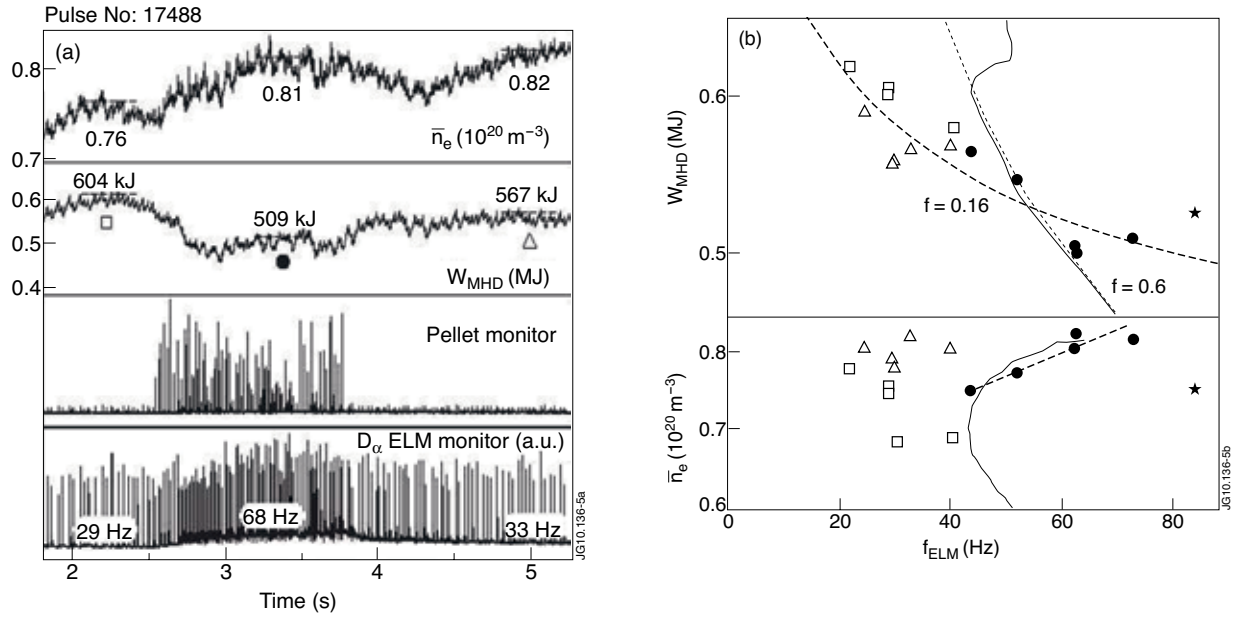

Figure 5: (a) Temporal evolution of plasma density, stored energy, pellet and ELM monitor signals in a type-I ELMy discharge containing a pellet pace making sequence (averaged ~ = 68Hz) and fuelling rate of ~17×10^{20}Ds^{-1}. (b) Data compiled from pellet injection frequency scan showing a mild degradation of con¯nement with increasing ELM frequency for pellet pace making. From reference [33].

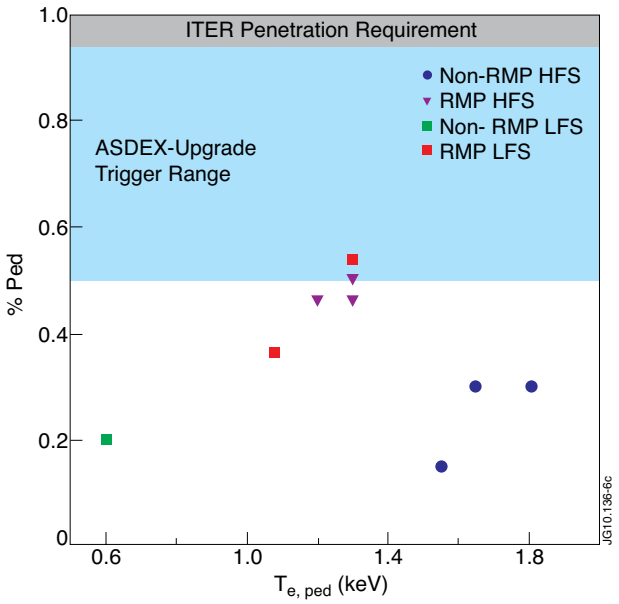

Figure 6: The pellet position where an ELM is triggered, plotted as a fraction of the pedestal height, vs the pedestal temperature measured from DIII-D discharges. All the pellets are 1.8mm and injected from either the inner wall (HFS) or outside midplane (LFS). From reference [36].

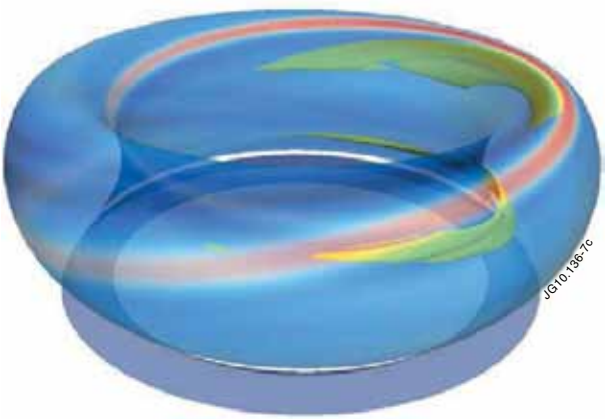

Figure 7: The temperature on a flux surface just inside the separatrix. The density contour of twice the central density is shown in yellow. The initial density perturbation was injected in the pedestal on the left-hand side in the figure. From reference [39].

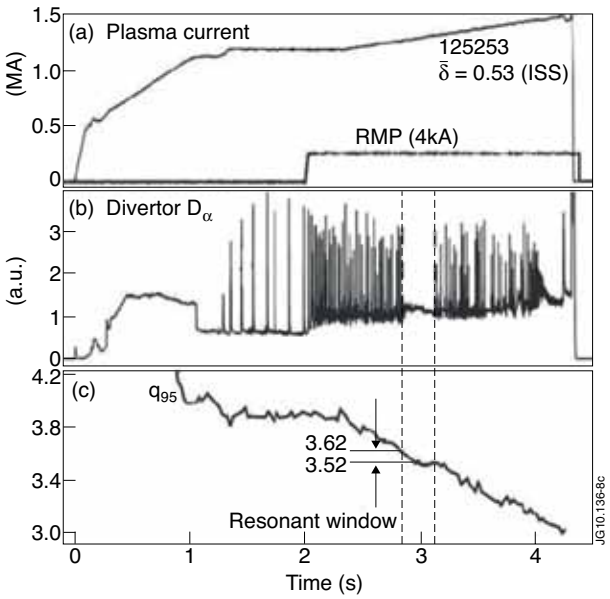

Figure 8: (a) Plasma and I-coil current, (b) lower divertor D_α signal showing ELM suppression window and (c) q_{95} resonant window during a 4kA RMP pulse in an ITER similar shape plasma with an average triangularity of 0.53 from a DIII-D ELM control discharge #125253). From reference [42].

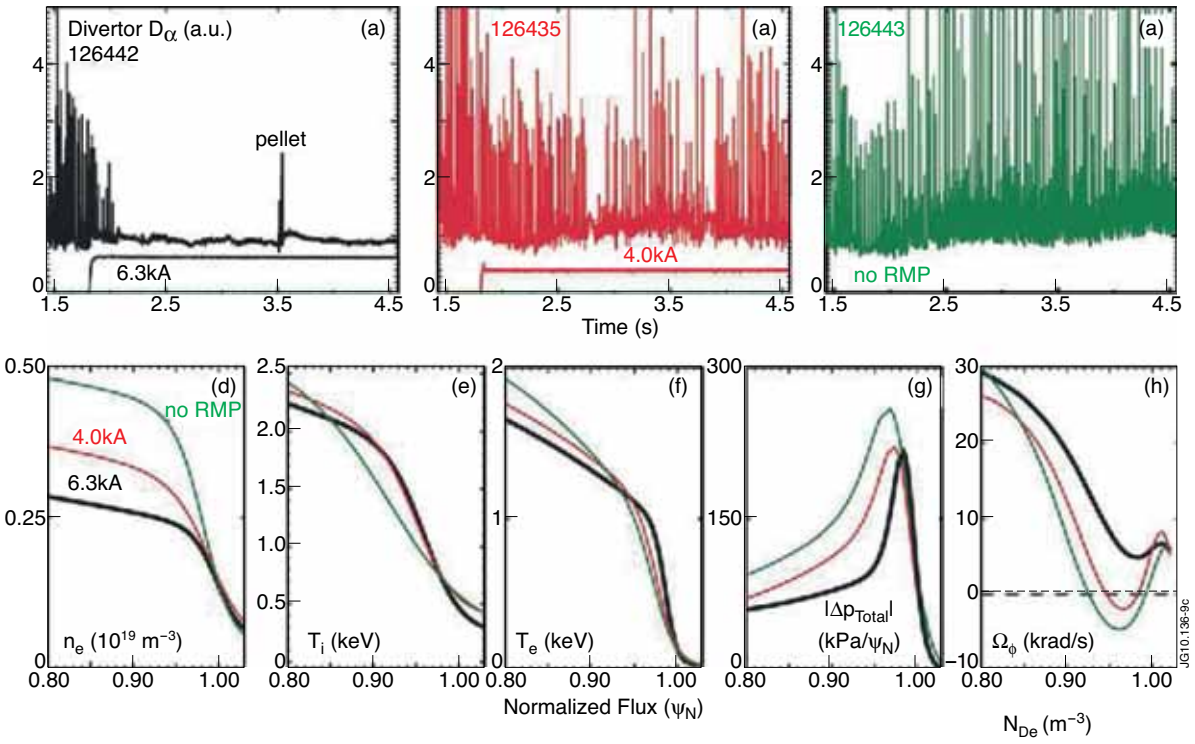

Figure 9: Lower divertor D_α signals showing the ELM characteristics in similar ISS plasmas with n = 3 I-coil currents of (a) 6.3 kA, (b) 4.0kA and (c) 0 kA. Pedestal pro¯les showing the (d) density, (e) ion temperature, (f) electron temperature, (g) absolute value of the total pressure gradient and (h) C6+ toroidal rotation for the three I-coil currents shown in (a), (b) and (c) where black, red and green correspond to 6.3kA, 4.0kA and 0kA, respectively. From reference [42].

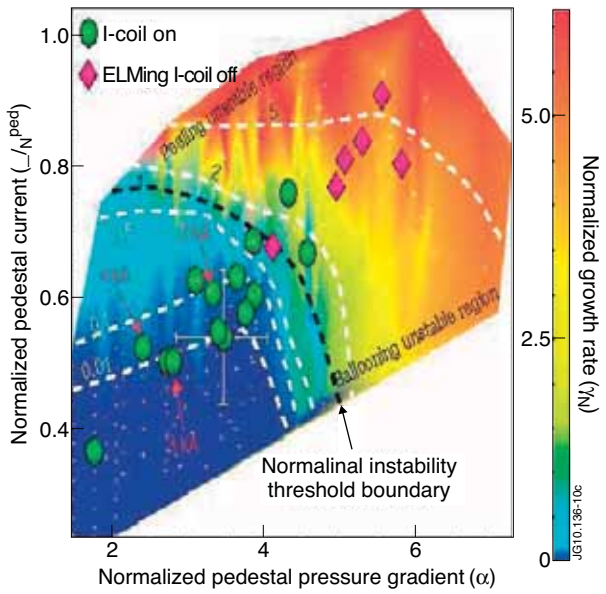

Figure 10: The normalized Peeling-Ballooning mode growth rates of an ELM unstable H-mode plasma (magenta diamonds) and RMP-induced ELM-free (green ellipses) plasma. From reference [41].

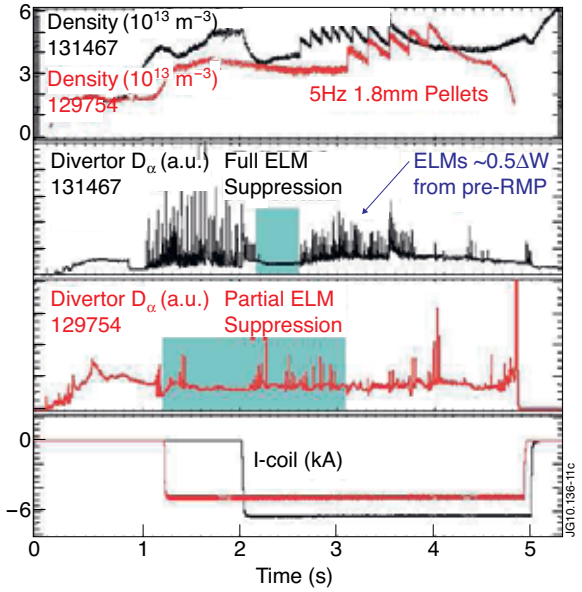

Figure 11: Two cases of 1.8mm fueling pellets injected from the inner wall into H-mode plasmas with RMP applied. In the full ELM suppressed case with 10Hz pellets, frequent ELMs are observed after the pellets start. The partial ELM suppressed case (lower coil current) shows only a few ELMs with the 5;Hz pellets. From reference [36].

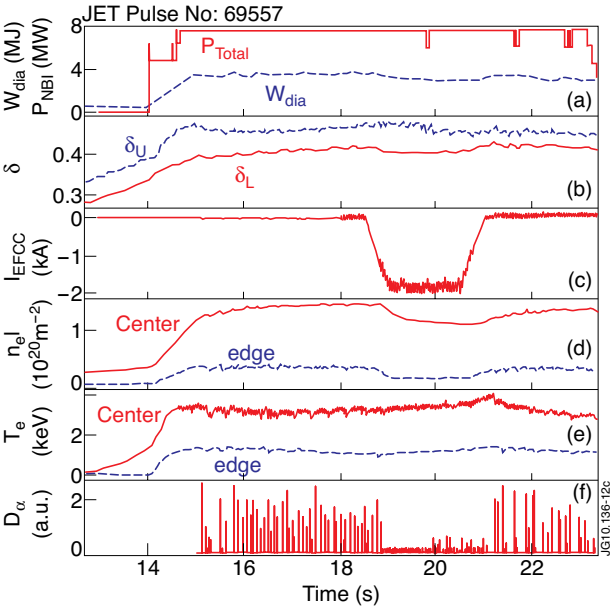

Figure 12: Overview on a typical ELM control experiment on JET . From reference [58].

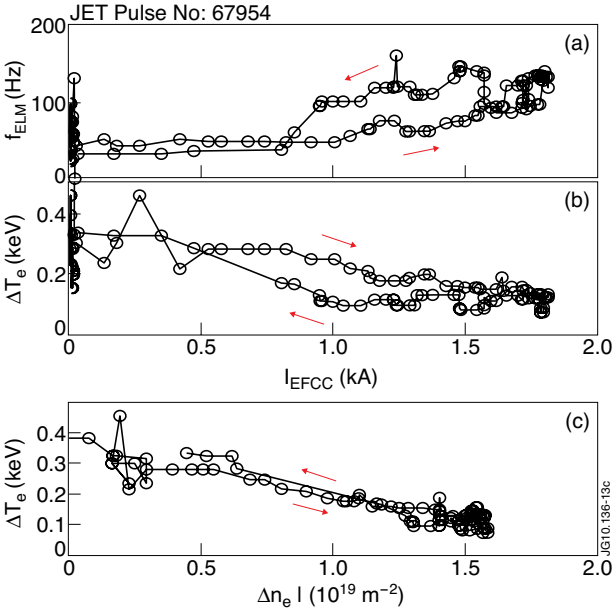

Figure 13: (a) Frequency of the ELMs, f_{ELM}, and (b) the amplitude of ΔT_e as a function of IEFCC. (c) Dependence of ΔT_e on the density drop due to the pump-out effect. From reference [54]